energy&fuels

Article

Cite This: Energy Fuels 2018, 32, 12198−12204

pubs.acs.org/EF

Analysis of Petroleum Products by Gel Permeation Chromatography Coupled Online with Inductively Coupled Plasma Mass Spectrometry and Offline with Fourier Transform Ion Cyclotron Resonance Mass Spectrometry

Jonathan C. Putman,[†,‡,§,∥,⊥] Sara Gutiérrez Sama,[§,∥,⊥] Caroline Barrère-Mangote,[§,∥] Ryan P. Rodgers,[†,‡,#] Ryszard Lobinski,[§,⊥] Alan G. Marshall,[*,†,‡] Brice Bouyssière,[*,§,⊥] and Pierre Giusti[§,∥]

[†]National High Magnetic Field Laboratory, Florida State University, 1800 East Paul Dirac Drive, Tallahassee, Florida 32310, United States

[‡]Department of Chemistry and Biochemistry, 95 Chieftain Way, Florida State University, Tallahassee, Florida 32306, United States

[§]TOTAL RC − CNRS Joint Laboratory C2MC, Complex Matrices Molecular Characterization, BP 27, 76700 Harfleur, France

[∥]TOTAL Raffinage Chimie, TRTG, BP 27, 76700 Harfleur, France

[⊥]CNRS/UNIV PAU & PAYS ADOUR/E2S UPPA, Institut Des Sciences Analytiques Et De Physico- Chimie Pour L'Environnement Et Les Materiaux, UMR5254, HELIOPARC- 2 Avenue du Président Angot, 64000 Pau, France

[#]Future Fuels Institute, Florida State University, 1800 East Paul Dirac Drive, Tallahassee, Florida 32310, United States

ABSTRACT: We have examined the aggregation behavior of a typical atmospheric residue feedstock by gel permeation chromatography (GPC). The size profiles for compounds containing sulfur, vanadium, and nickel were determined online from elemental detection by inductively coupled plasma (ICP) mass spectrometry. Four fractions that vary in aggregation state were analyzed by positive atmospheric pressure photoionization (APPI) 9.4 T Fourier transform ion cyclotron resonance mass spectrometry (APPI FT-ICR MS). Results showed an inverse relationship between fraction aggregate size and monomer ion yield and revealed that aggregation tendency did not correlate with higher polar or aromatic species abundance. Aggregation in the atmospheric residue more closely correlated with increased relative abundance of larger and more aliphatic compounds. The molecular composition of the GPC aggregate fractions suggests that nonpolar intermolecular forces between saturated, long-chain alkyl substituents contribute more to aggregation than pi−pi interactions.

INTRODUCTION

Heavy metals in crude oils and petroleum distillates can cause complications in refinery processes due to deactivation of hydrotreatment and hydrocracking catalysts. The most abundant metals, such as vanadium, nickel, and iron, exist as heterocyclic macrocycles containing four modified pyrrole subunits (porphyrins). Petroporphyrins provide clues about the geochemical origin of a crude oil, and knowledge of the size distributions of metalloporphyin aggregates enables better optimization strategies in the refinery process, rather than relying solely on total metal concentration.[1,2]

Gel permeation chromatography (GPC) with elemental detection by inductively coupled plasma mass spectrometry (ICP MS) enables determination of size profiles for species that contain heavy metals. It is well-known that metal-containing petroporphyrins are involved in macromolecular aggregation with asphaltenes, but the forces driving asphaltene precipitation and its relationship to on-column aggregation during GPC separations are not well understood.[3] Element-specific aggregate size distributions also provide unique fingerprints for petroleum samples.[4,5] GPC chromatograms for porphyrinic metals, such as vanadium and nickel, often exhibit multimodal (typically trimodal) distributions. The multimodal GPC profiles can aid in the determination of fraction cut-points. Traditionally, GPC profiles for porphyrinic metals are divided into four main fractions to probe various aggregation states. In recent years, significant effort has been made to determine the significance of GPC ICP MS results with regard to specific problems in the refinery and upgrading processes. The technique has been applied to distillation cuts[4] and isolated interfacial material,[6] as well as saturates, aromatics, resins, and asphaltenes fractions.[5,7] Often the determination of a true molecular mass distribution by GPC is very difficult. Optimization of refinery processes, such as hydrogenation, catalytic cracking, and coking, requires detailed molecular-based compositional analysis. GPC size distributions for petroleum products that received various upgrading treatments can provide insight into the process efficacy.[8] Often, upgrading and treatment processes have clear differences in conversion efficiency across the GPC molecular weight distribution.[7] To truly gauge the significance of GPC results and maximize improvements to refinery techniques, the molecular-level

Received: August 13, 2018
Revised: October 30, 2018
Published: October 30, 2018

DOI: 10.1021/acs.energyfuels.8b02788
Energy Fuels 2018, 32, 12198−12204

composition must be understood as a function of aggregation potential. Without detailed molecular characterization, it is nearly impossible to understand how aggregation depends on molecular structure.

Previous GPC studies with molecular-level characterization are scarce but have provided some important observations about the elution behavior of petroleum products that should be taken into consideration when interpreting results. Ideally, elution in GPC separations should be dictated solely by differences in hydrodynamic volume.[9] Very often, however, clear signs of analyte adsorption to the column packing material have been observed. In the analysis of coal tar pitch by Hansen et al., the peak maxima occurred after the total permeation limit with tetrahydrofuran (THF) as the mobile phase.[8] Another study that utilized THF observed the separation of compounds with the same aromatic core and varying alkyl carbon chain length. The results showed that retention time and the degree of alkylation were inversely correlated.[10] Assuming that interactions with the column packing material are minimal, or at least not strong enough to affect elution order, these results could indicate that increased aliphaticity contributes to aggregation potential. Indeed, it has been shown that unstable asphaltenes have higher capacity for binding to alkanes and waxes.[11] In the analyses of asphaltenes, petroleum pitch, and coal-derived materials, increased molecular weight of the GPC fractions correlated with decreases in fluorescence intensity and UV absorbance.[8,12,13] Berrueco et al. also observed enrichment in the high molecular weight, excluded peak of an n-methylpyrrolidine-insoluble subfraction from an asphaltene, and they hypothesized that the excluded peak was likely composed of species that were larger in molecular size and more aliphatic in nature.[13] In practice, interactions with the stationary phase can never be completely eliminated,[14,15] but certainly the mobile phase and column conditions should minimize interferences from effects not related to hydrodynamic volume.

The work herein utilizes high resolution mass spectrometry to observe changes in molecular composition across a GPC elution profile. For all mass spectral analyses, the ionization process plays an important role in which compounds are detected. For complex mixtures, the choice of ionization method is especially important, because differences in ionization efficiency and aggregation state between chemical species can result in preferential detection of the most easily ionized compounds. Here, we chose positive-ion APPI because it is widely thought to be the most suitable ionization process for the analyses of asphaltenes.[16−18] Compared to electrospray, APPI results in more uniform ionization efficiency; however, the preferential ionization of aromatics by APPI is well documented.[16,19] In this work, discrepancies arising from ionization biases were minimized by fractionation.[20,21] Four GPC fractions of various aggregate sizes were collected from a refinery atmospheric residue feedstock produced from a typical, middle-eastern crude oil. The fractions were then analyzed by APPI 9.4 T Fourier transform ion cyclotron resonance mass spectrometry (FT-ICR MS) to probe chemical composition as a function of aggregation potential.

EXPERIMENTAL METHODS

Instrumentation and Materials. The GPC separation was performed with an AKTA*purifier* liquid chromatography system equipped with a UV-900 multiwavelength UV absorbance detector and a Frac-950 fraction collector (GE Healthcare Bio-Sciences, Pittsburgh, U.S.A.). Three polymeric Shodex preparative GPC columns (see Table 1) were connected in series (KF-2004, KF-2002.5, and KF-2001; Showa Denko America, Inc., New York, U.S.A.) as shown in Figure 1. The mobile phase consisted of 100% ACS reagent grade xylene (Scharlab,S.L., Gato Pérez, Barcelona, Spain). Preparative-scale separations were performed at a flow rate of 3 mL/min. A large postcolumn split allowed most of the eluent to be sent to the fraction collector. The low-flow outlet from the splitter (~40 μL/min) was directed to a Thermo Scientific Element XRsector field ICP-HRMS instrument. The GPC-ICP interface and the ICP experimental conditions have been described previously.[4,5] Briefly, ^{32}S, ^{51}V, and ^{58}Ni isotopes were monitored online at medium resolution (mass resolving power = 4000). A modified DF-5 microflow total consumption nebulizer (CETAC, Omaha, NE) fitted to the front end of the MS facilitated sample introduction. The temperature of the spray chamber was maintained at 60 °C by a Neslab RTE-111 temperature-controlled bath circulator (Thermo Fisher Scientific, Waltham, MA).[22,23]

Table 1. Column Details

column no.	GPC column ID (standard/prep.)	exclusion limit (polystyrene MW)	pore size (Å)	particle size (μm)
1	K-804/KF-2004	400 000	1500	7
2	K-802.5/KF-2002.5	20 000	300	6
3	K-801/KF-2001	1500	50	6

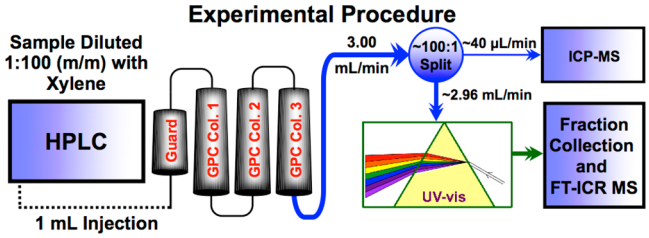

Figure 1. Experimental event sequence for preparative-scale GPC separations with fraction collection and online detection by ICP-MS and UV−visible spectroscopy.

The collected fractions were analyzed by positive APPI with a custom-built 9.4 T FT-ICR mass spectrometer.[16,24,25] The APPI source (ThermoFisher Scientific, San Jose, CA) was interfaced to the front stage of the mass spectrometer with a custom-built adapter.[26] The vaporization temperature of the source was set to 350 °C, and N_2 was used as the sheath gas (50 psi) and the auxiliary gas (32 mL/min) to avoid sample oxidation. All samples and fractions were dissolved in toluene at a concentration of 100 μg/mL, and direct infusion experiments were performed at a flow rate of 50 μL/min. For each sample, 100 time-domain transients with six second acquisition period were coadded, Hanning-apodized, and zero-filled once prior to Fourier transform and broadband phase correction[27] to yield absorption-mode FT-ICR mass spectra with resolving power greater than 1 100 000 at m/z 500. Calibration and data processing were performed by use of Predator Analysis and PetroOrg.[25,28]

RESULTS AND DISCUSSION

Aggregate Size Distributions for Sulfur, Vanadium, and Nickel. During the GPC separation, ^{32}S, ^{51}V, and ^{58}Ni isotopes were monitored online by ICP MS. The mass chromatograms in Figure 2 show that sulfur-containing compounds elute in a single broad peak with a monomodal distribution, whereas compounds that contain vanadium or nickel exhibit a trimodal distribution. One possible explanation for the observed multimodal distributions is compositional

DOI: 10.1021/acs.energyfuels.8b02788
Energy Fuels 2018, 32, 12198−12204

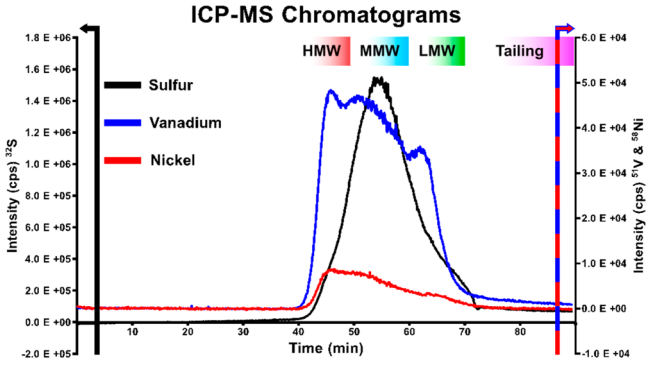

Figure 2. GPC ICP mass chromatograms for a typical atmospheric residue feedstock. Sulfur intensity is plotted on the primary axis, and the heavy metals' intensities correspond to the secondary axis on the right. Vanadium and nickel chromatograms exhibit a trimodal distribution. In contrast, the sulfur chromatogram shows only one peak centered in the medium molecular weight aggregate fraction.

changes in the compounds that elute in each region that contribute to differences in aggregation potential. To probe this possibility, fractions corresponding to the multimodal mass profile were collected for further analyses. The collected fractions were evaporated dry, diluted, and reinjected to determine the reproducibility and the stability of their aggregate size distributions. For compositional characterization, the fractions were then analyzed by FT-ICR MS.

Aggregation Reproducibility for Collected Fractions. To determine the stability of the aggregation tendency, fractions that correspond to the valleys in the multimodal mass distributions were collected for reinjection. The fractions were diluted 1:100 (m/m) prior to reinjection. The constant dilution factor for both the sample and the collected fractions leads to reinjection of the fractions at higher concentrations than that of the whole atmospheric residue. Based on the mass balance in Table 2, the concentration of the reinjected medium MW fraction was ~1.5 times greater than for initial injection of the whole sample, whereas the low molecular weight and high molecular weight fractions were reinjected at ~5 times greater relative concentrations. Figure 3 shows the sulfur and vanadium ICP-MS chromatograms for the whole sample and its reinjected fractions. Upon reinjection, all three MW GPC fractions demonstrated stable aggregation potentials and eluted in their respective MW bins. The constant dilution factor provides a probe to differentiate composition-driven aggregation from concentration-driven aggregation. For the high and medium MW fractions, stable retention times should be expected. If there are larger aggregates in the high MW fraction due to the higher reinjected concentration, they would be unobservable, as the high MW fraction already elutes near the total exclusion limit of the GPC column. Reinjection concentration should also have minimal effect on the medium MW fraction, which was reinjected at only 1.5× higher concentration. However, the reinjection of the low MW fraction, shown in green, provides the most conclusive inferences. The signal stays very close to baseline and very little low MW material elutes at retention times less than 30 min. Most of the low MW peak area in both chromatograms elutes within the low MW bin. These observations rule out the possibility of purely concentration-driven aggregation and provide evidence that the fractions are composed of distinctly different compounds. In a scenario with purely concentration-driven aggregation, all of the fractions would contain the same compounds acting as monomers. In that case, higher concentration would lead to larger, multimeric aggregates, and one would expect to observe significant decrease in retention times for the reinjected fractions, especially for the low MW fraction. Therefore, we can conclude with certainty that aggregation potential must be driven, at least in part, by chemical composition. Furthermore, in the case of aggregation during GPC separations, we can infer that chemical composition likely contributes more significantly to aggregation potential than concentration.

Characterization of Aggregate Fractions by FT-ICR MS. Further characterization of the atmospheric residue and its GPC fractions was performed by positive APPI 9.4 T FT-ICR MS, and Figure 4 shows the broadband mass spectra. The top of Figure 4 shows the broadband mass spectrum for the whole sample, showing characteristics typical of an atmospheric-residue feedstock. The mass distribution is centered at $m/z \approx 400$, and ~16 000 elemental compositions were assigned. Several interesting trends were observed in the broadband mass spectra for the tailing, low MW, medium MW, and high MW, shown in descending order, with the high MW fraction at the bottom of Figure 4. First, the average MW of the mass distributions increases with the fraction aggregate sizes measured by GPC. The mass distribution of tailing fraction exhibits a lower average MW than the whole sample, and the highest magnitude peaks are at $m/z < 300$. The mass spectrum for the low MW fraction is centered at $m/z \approx 300-325$, and the medium MW fraction has a broadband centered at $m/z \approx 400$. The correlation between aggregation potential measured by GPC and the average molecular weight in the mass spectra indicates aggregation based on chemistry rather than concentration. Aggregation based solely on concentration would yield fractions with same chemical species acting as monomers to combine into multiple aggregation states. However, Figure 4 clearly shows that even out of the aggregated state, each fraction is composed of chemically different species. With the exception of the high MW fraction, the other broadband mass spectra have monomodal, pseudo-Gaussian distributions, which is typical for petroleum samples. However, the high MW fraction (Figure 4, bottom) has a multimodal, atypical mass distribution that extends out to at least m/z 1500. The number of assigned peaks reveals a relationship between aggregation potential and complexity.

Table 2. Average and %RSD for the Mass Recovery and Area Distributions from the Atmospheric Residue Sample (n = 5)

fraction	mass recovery (%)		^{32}S area (%)		^{51}V area (%)		^{58}Ni area (%)	
high M.W.	15.2	±2.9	13.9	±0.3	30.1	±1.6	35.1	±1.6
medium M.W.	75.7	±7.3	59.6	±2.2	44.7	±0.4	42.1	±2.1
low M.W.	8.2	±6.1	21.4	±0.4	22.2	±0.7	18.8	±0.4
tailing	0.9	±1.6	5.1	±2.2	3.0	±1.2	4.1	±2.8
total	100.9	±15.0	100		100		100	

DOI: 10.1021/acs.energyfuels.8b02788
Energy Fuels 2018, 32, 12198−12204

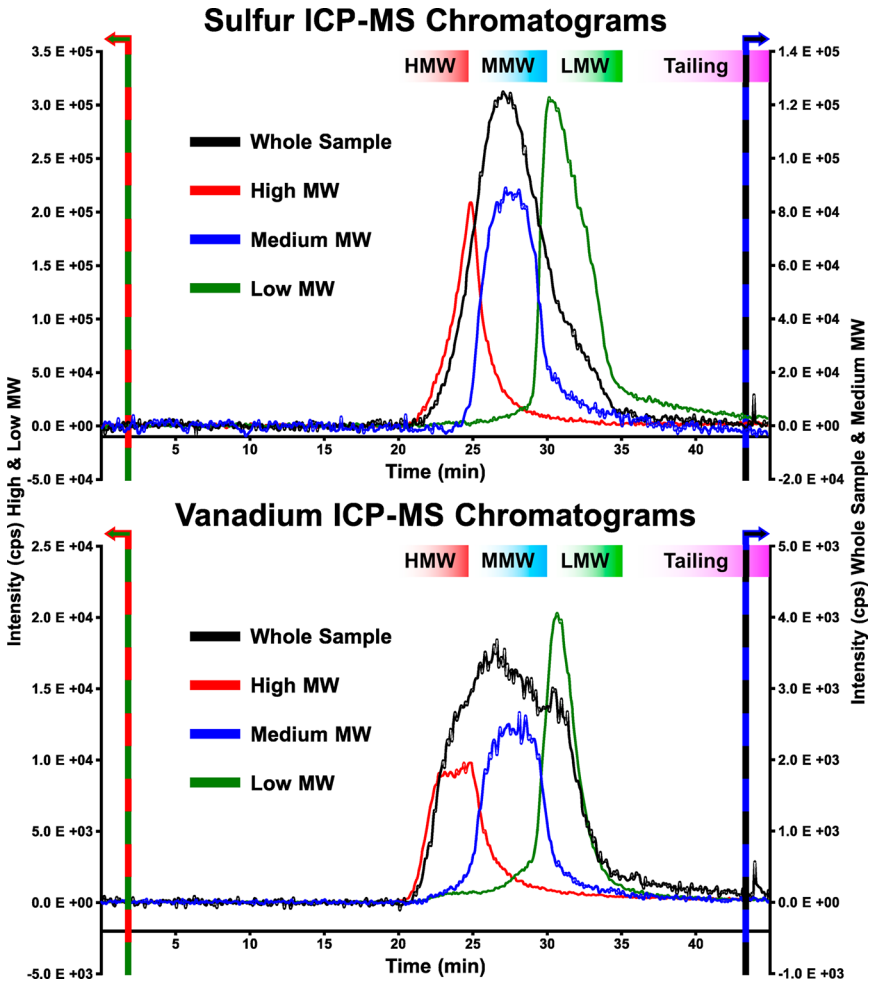

Figure 3. Sulfur (left) and vanadium (right) GPC ICP mass chromatograms for the atmospheric residue and its reinjected fractions. The primary axis corresponds to the signal from the reinjected high M.W. and low M.W. fractions, while the secondary axis corresponds to the whole sample and reinjected medium M.W. fraction.

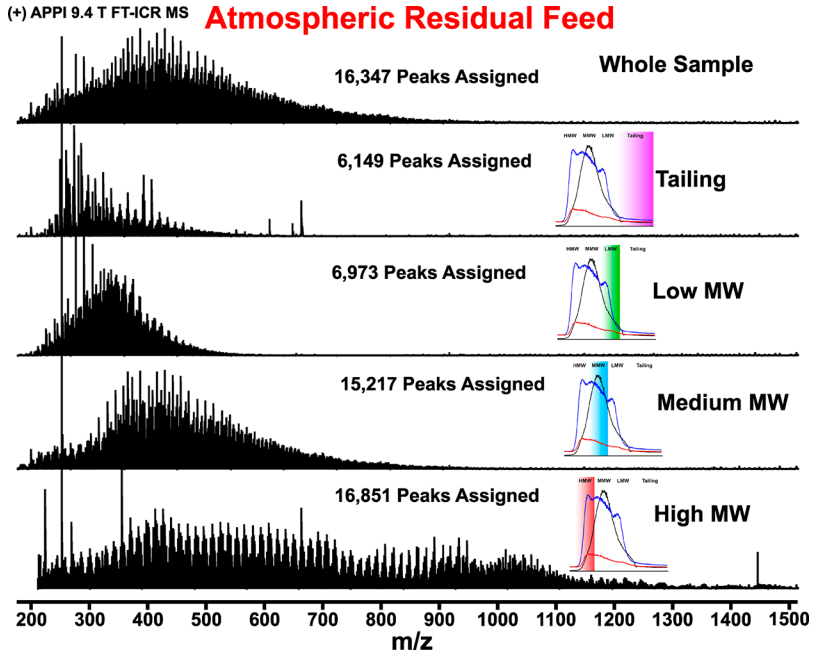

Figure 4. Positive ion atmospheric pressure photoionization (APPI) broadband 9.4 T FT-ICR mass spectra for the feedstock atmospheric residue and its aggregate fractions.

DOI: 10.1021/acs.energyfuels.8b02788
Energy Fuels 2018, 32, 12198−12204

The high MW fraction exhibits the greatest complexity with ~17 000 assigned peaks, and the tailing fraction has the least complexity with ~6000 assigned peaks.

The heteroatom class distributions for the whole sample and its GPC fractions are shown in Figure 5. In the whole

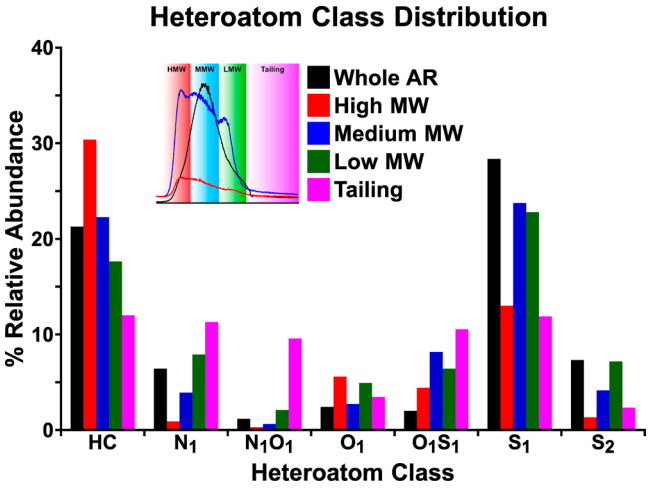

Figure 5. Heteroatom class distributions from (+) APPI 9.4 T FT-ICR mass spectral analysis of the atmospheric residue feedstock and its corresponding GPC fractions.

atmospheric residue feedstock, the sulfur (S_1) and hydrocarbon (HC) classes have the highest relative abundance (~30% and ~20%). In the GPC fractions, the HC class abundance shows a strong correlation with aggregation potential and is the most abundant in the largest, high MW aggregate fraction. However, the S_1 class abundance did not depend on aggregation state and is highest for the medium and low MW fractions. The relative abundance of the sulfur class is distributed across the fractions as one would expect based on the total sulfur ICP MS chromatogram and in accordance with the total mass yields shown in Table 2.

Figure 6 (left) shows the average H/C ratios for the heteroatom class families. The H/C ratio gives a measure to the degree of saturation; greater H/C ratio correlates with more aliphatic species and smaller H/C ratio with more aromatic type components. The average H/C ratios show a surprisingly strong correlation between aromaticity and aggregation potential. As aggregate size increases, the molecular composition of the fractions becomes increasingly aliphatic. In each of the six most abundant heteroatom class families, the high MW fraction (as measured by GPC) has the highest average H/C ratio (most saturated). Furthermore, a significant decrease in the average H/C ratio was observed for the least aggregated, tailing, and low MW fractions. Together, these results indicate that pi−pi interactions between highly aromatic species are not a major driving force behind aggregation: rather, weaker, nonpolar intermolecular forces between saturated, long-chain alkyl substituents contribute more to the aggregation that occurs on a GPC column.

Figure 6 (right) reinforces these speculations, based on the monomer ion yields for the GPC fractions. Monomer ion yield reflects the relative ionization efficiency for each fraction. Monomer ion yield was calculated from the inverse of the ion accumulation period used to collect the FT-ICR mass spectra, as previously reported.[29] These values were then normalized to the tailing fraction, and show an inverse relationship between

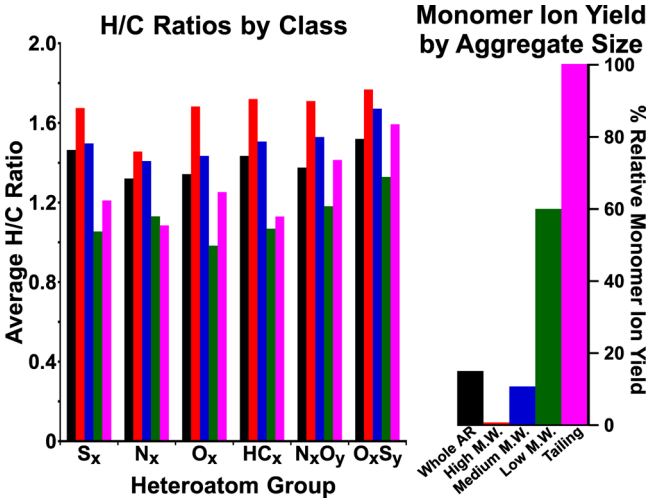

Figure 6. Left: Average H/C ratios of the heteroatom class groups, showing that as aggregate size increases, the molecular composition of the fractions becomes increasingly aliphatic. For each of the six most abundant heteroatom groups, the high molecular weight fraction (as measured by GPC) has the highest average H/C ratio (most saturated). Right: Monomer ion yield for the atmospheric residue and its fractions.

monomer ion yield and aggregate size. Whereas monomer ion yield provides only a qualitative value for ionization efficiency, the trend is undeniable. On the two extreme ends of the range, the tailing fraction required accumulation periods of ~1−5 ms, vs 10−20 s for the high MW fraction. One would expect aromatic and polar compounds to ionize most efficiently by (+) APPI, so these results corroborate the inferences made from the average H/C ratios in Figure 6 (left).

Molecular Composition of Aggregate Fractions. Molecular level characterization further supports the relationship between decreased aromaticity and aggregation potential. Figure 7 consists of isoabundance-contoured plots of double bond equivalents (DBE = number of rings plus double bonds to carbon) vs carbon number for the HC (top) and S_1 (bottom) heteroatom classes. On the far left, the plots for the whole sample occupy a fairly typical compositional space for an atmospheric residue, with an average carbon number of ~37 and an average DBE of ~12−13 for both classes. For the tailing fraction on the far right, the average DBE is significantly greater than for the whole sample. The compositional range coverage for the tailing distributions also shifts dramatically. For both classes the most abundant hotspots are highly aromatic and occupy locations very close to the polycyclic aromatic hydrocarbon (PAH) planar limit, indicated by the red dashed lines.[30,31] The low MW GPC fraction also contains highly aromatic species, but the distribution is slightly displaced from the PAH planar limit. The medium MW fractions, shown in the middle of Figure 7, occupy a compositional range similar to that for the whole sample. The average carbon number and average DBE of the medium MW fractions are approximately the same as the whole sample. The only major difference between the medium MW fractions the whole sample is the absence of the most condensed aromatic compounds, which eluted in the tailing and low MW fractions. The high MW fraction continues the observed trends, and the distribution is significantly displaced from the PAH planar limit. Compared to the whole sample, the average DBE is lower, and the average carbon number is higher (~67

DOI: 10.1021/acs.energyfuels.8b02788
Energy Fuels 2018, 32, 12198−12204

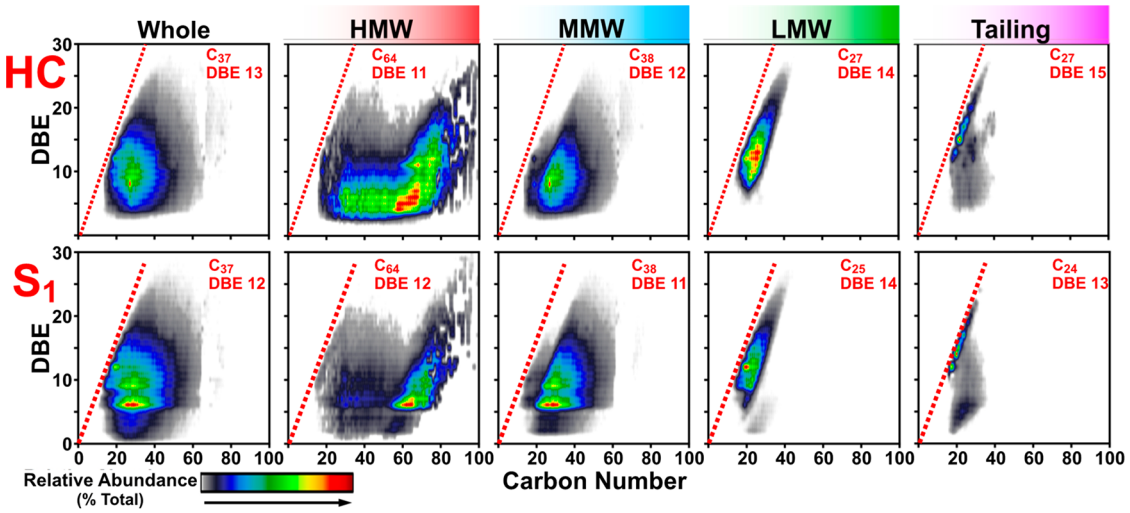

Figure 7. Positive ion APPI-derived isoabundance-contoured plots of double bond equivalents vs carbon number for the HC class (top) and S_1 class (bottom). The red dashed lines represent the polycyclic aromatic hydrocarbon planar limit.

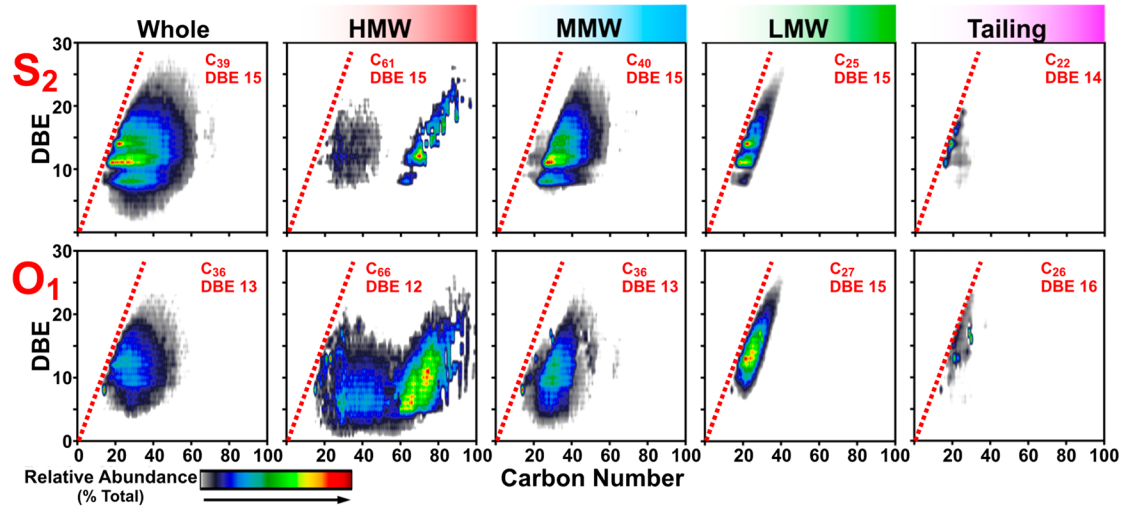

Figure 8. Positive ion APPI-derived isoabundance-contoured plots of double bond equivalents vs carbon number for the S_2 class (top) and O_1 class (bottom). The red dashed lines represent the polycyclic aromatic hydrocarbon planar limit.

vs ~34)). For both the HC class and the S_1 class, the most abundant hotspots are in the range of 60−70 carbons and a DBE of 4−6. The compositional range corresponds to compounds with 1−3 aromatic rings and 60−70 total carbon atoms; these species are likely highly aliphatic with very long alkyl chains. The same observations discussed above were made for all of the other most abundant heteroatom classes, two of which (S_2 and O_1) are shown in Figure 8.

CONCLUSIONS

As the aggregation state measured by GPC grows larger, complexity and the average molecular weight of the mass distribution both increase. Fraction aggregate size and monomer ion yield were found to be inversely related, as shown by the trend in Figure 6, and the most aggregated GPC fraction contained compounds with very low ionization efficiencies. For the most abundant heteroatom classes, the most aggregated fraction had the lowest average DBE and at the same time the average carbon number was almost two times greater than that of the whole sample. Contrary to expectation, aggregation dependence did not correlate with higher relative abundance of polar or polyaromatic species. Thus, the results suggest that aggregation tendency (~or behavior) correlates with weaker, nonpolar intermolecular forces between saturated, long-chain alkyl substituents. Ongoing work focuses on determining the significance of that finding with regard to asphaltene precipitation and the aggregation of petroleum products during refinery processes.

AUTHOR INFORMATION

Corresponding Authors

*Tel: 1-850-644-0529. Fax: 1-850-644-1366. E-mail: marshall@magnet.fsu.edu.

*Tel: +33 (0) 559 407 752. Fax: +33 (0) 559 407 781. E-mail: brice.bouyssiere@univ-pau.fr.

ORCID

Ryan P. Rodgers: 0000-0003-1302-2850

Alan G. Marshall: 0000-0001-9375-2532

Brice Bouyssière: 0000-0001-5878-6067

Pierre Giusti: 0000-0002-9569-3158

DOI: 10.1021/acs.energyfuels.8b02788
Energy Fuels 2018, 32, 12198−12204

Notes

The authors declare no competing financial interest.

■ ACKNOWLEDGMENTS

Work supported by National Science Foundation Cooperative Agreements No. DMR-11-57490 and DMR-1644779, the State of Florida, Conseil Régional d'Aquitaine (20071303002PFM), and FEDER (31486/08011464). The authors thank TOTAL for supplying oil samples and Steven M. Rowland for helpful discussions and feedback.

■ REFERENCES

(1) Xu, H.; Que, G.; Yu, D.; Lu, J. R. *Energy Fuels* **2005**, *19* (2), 517−524.
(2) López, L.; Lo Mónaco, S.; Richardson, M. *Org. Geochem.* **1998**, *29* (1-3), 613−629.
(3) Gascon, G.; Vargas, V.; Feo, L.; Castellano, O.; Castillo, J.; Giusti, P.; Acavedo, S.; Lienemann, C. P.; Bouyssiere, B. *Energy Fuels* **2017**, *31* (8), 7783−7788.
(4) Desprez, A.; Bouyssiere, B.; Arnaudguilhem, C.; Krier, G.; Vernex-loset, L.; Giusti, P. 2014.
(5) Gutierrez Sama, S.; Desprez, A.; Krier, G.; Lienemann, C.-P.; Barbier, J. J.; Lobinski, R.; Barrere-Mangote, C.; Giusti, P.; Bouyssiere, B. *Energy Fuels* **2016**, *30* (9), 6907−6912.
(6) Ligiero, L. M.; Bouriat, P.; Dicharry, C.; Passade-Boupat, N.; Lalli, P. M.; Rodgers, R. P.; Barrère-Mangote, C.; Giusti, P.; Bouyssiere, B. *Energy Fuels* **2017**, *31* (2), 1065−1071.
(7) Cui, Q.; Nakabayashi, K.; Ma, X.; Miyawaki, J.; Al-mutairi, A.; Marafi, A. Mj.; Park, J.; Yoon, S.; Mochida, I. *Energy Fuels* **2017**, *31* (7), 6637.
(8) Hansen, B. E.; Malmros, O.; Turner, N. R.; Stenby, E. H.; Andersen, S. I. *Proc. Light Metals; New Orleans, LA* **2001**, 559−564.
(9) Lathe, G. H.; Ruthven, C. R. J. *Biochem. J.* **1956**, *62* (4), 665−674.
(10) Molnárné Guricza, L.; Schrader, W. *Fuel* **2018**, *215* (215), 631−637.
(11) Orea, M.; Ranaudo, M. A.; Lugo, P.; López, L. *Energy Fuels* **2016**, *30* (10), 8098−8113.
(12) Lazaro, M. J.; Islas, C. A.; Herod, A. A.; Kandiyoti, R. *Energy Fuels* **1999**, *13* (6), 1212−1222.
(13) Berrueco, C.; Venditti, S.; Morgan, T. J.; Álvarez, P.; Millan, M.; Herod, A. A.; Kandiyoti, R. *Energy Fuels* **2008**, *22* (5), 3265−3274.
(14) Sato, S.; Takanohashi, T. *Energy* **2005**, No. 10, 1991−1994.
(15) Prokai, L.; Simonsick, W. J., Jr. *Rapid Commun. Mass Spectrom.* **1993**, *7* (9), 853−856.
(16) McKenna, A. M.; Marshall, A. G.; Rodgers, R. P. *Energy Fuels* **2013**, *27* (3), 1257−1267.
(17) Itoh, N.; Aoyagi, Y.; Yarita, T. *J. Chromatogr. A* **2006**, *1131* (1−2), 285−288.
(18) Robb, D. B.; Covey, T. R.; Bruins, a. P. *Anal. Chem.* **2000**, *72* (15), 3653−3659.
(19) Andreatta, G.; Bostrom, N.; Mullins, O. C. *Langmuir* **2005**, *21* (7), 2728−2736.
(20) Chacón-Patiño, M. L.; Rowland, S. M.; Rodgers, R. P. *Energy Fuels* **2018**, *32* (1), 314−328.
(21) Rowland, S. M.; Robbins, W. K.; Corilo, Y. E.; Marshall, A. G.; Rodgers, R. P. *Energy Fuels* **2014**, *28* (8), 5043−5048.
(22) Giusti, P.; Nuevo Ordonez, Y.; Philippe Lienemann, C.; Schaumloffel, D.; Bouyssiere, B.; Lobinski, R. *J. Anal. At. Spectrom.* **2007**, *22* (1), 88−92.
(23) Caumette, G.; Lienemann, C.-P.; Merdrignac, I.; Paucot, H.; Bouyssiere, B.; Lobinski, R. *Talanta* **2009**, *80* (2), 1039−1043.
(24) Kaiser, N. K.; Quinn, J. P.; Blakney, G. T.; Hendrickson, C. L.; Marshall, A. G. *J. Am. Soc. Mass Spectrom.* **2011**, *22* (8), 1343−1351.
(25) Blakney, G. T.; Hendrickson, C. L.; Marshall, A. G. *Int. J. Mass Spectrom.* **2011**, *306* (2−3), 246−252.
(26) Purcell, J. M.; Hendrickson, C. L.; Rodgers, R. P.; Marshall, A. G. *Anal. Chem.* **2006**, *78* (16), 5906−5912.
(27) Xian, F.; Hendrickson, C. L.; Blakney, G. T.; Beu, S. C.; Marshall, A. G. *Anal. Chem.* **2010**, *82* (21), 8807−8812.
(28) Corilo, Y. E. *PetroOrg. Software*; Florida State University: Tallahassee, FL, 2017.
(29) Chacón-Patiño, M. L.; Rowland, S. M.; Rodgers, R. P. *Energy Fuels* **2017**, *31* (12), 13509−13518.
(30) Hsu, C. S.; Lobodin, V. V.; Rodgers, R. P.; McKenna, A. M.; Marshall, A. G. *Energy Fuels* **2011**, *25* (5), 2174−2178.
(31) Lobodin, V. V.; Marshall, A. G.; Hsu, C. S. *Anal. Chem.* **2012**, *84* (7), 3410−3416.

DOI: 10.1021/acs.energyfuels.8b02788
Energy Fuels 2018, 32, 12198−12204